Highly Stretchable Piezoresistive Graphene–Nanocellulose Nanopaper for Strain Sensors

*Chaoyi Yan, Jiangxin Wang, Wenbin Kang, Mengqi Cui, Xu Wang, Ce Yao Foo, Kenji Jianzhi Chee, and Pooi See Lee**

Strain sensors are used to detect the electrical shift upon mechanical deformations and have found broad applications in infrastructural and automobile health monitoring.[1] Existing commercial products are mainly based on bulky technologies which are cheap but can only detect low strains within a few percent due to the very limited stretchability of metal and semiconductors.[2,3] However, strain sensors that are capable for the detection of high strain (>50%) are of compelling interest for emerging applications such as human-friendly interactive electronics. For example, the movements of human joints will generate strains as high as 55% upon stretching and contracting,[4] which far exceeds the detection limit (ca. 5%) of conventional strain sensors. High-strain sensors are in imperative demands for unprecedented applications beyond the existing markets,[4] such as wearable health-monitoring patch, robotic sensory skin and tele-surgery electronic glove, which all require high-strain sensing capabilities that cannot be achieved by simple extension of conventional technology.

Nanoscale materials were shown to be promising building blocks for innovative strain sensors with enhanced performances, and devices based on several representative nanostructures such as nanoparticles,[5] nanowires,[6] nanotubes[4] and graphene[7] have been reported. Especially, graphene nanosheets with extraordinary electrical and mechanical properties[8–11] have been extensively studied for strain sensing applications.[12–18] Piezoresistive monolayer and few-layer graphene has been used for strain detection,[12,14,15,17,18] however, the graphene layers can only be stretched to a very limited extent ca. 6%.[15] Proper structural design such as creating buckled structures for originally rigid materials, a strategy that has been widely used for stretchable electronics,[19,20] can be employed to improve the stretchability of graphene to 25–30%,[15,16] which unfortunately is still unsatisfying for efficient human-motion detection where the maximum strain exceeds 50%.

The development of high-strain graphene sensors remains technically challenging. In this report, we present an innovative strategy to fabricate graphene sensors with detection limit up to 100%. Three-dimensional (3D) macroporous nanopapers composed of crumpled graphene and nanocellulose were embedded in stretchable elastomer matrix to fabricate the strain sensors. To date, very limited reports on graphene sensors with stretchability above 50% can be found. Chen et al. reported the fabrication of 3D graphene foams by growing graphene on copper or nickel foam substrate and then etching away the metal template.[13] The graphene foam embedded in elastomer can be stretched to 95% before mechanical fracture. Excellent stretchability was achieved despite that the method requires high-cost chemical vapor deposition (CVD) growth and time-consuming etching processes.[13] With the ever-increasing demands of facile, low-cost and scalable nanofabrication techniques, developments of alternative routes to graphene high-strain sensors are of growing interest. Herein we suggest that our methods based on solution-processable graphene are significantly advantageous than the previous method in terms of fabrication complexity, production costs and scalability. The present methodology developed paves the way for practical applications of high-performance graphene-based piezoresistive devices.

Fabrication processes of the graphene nanopapers are shown in **Figure 1**a. Flexible nanopapers based on crumpled graphene and nanocellulose were first fabricated and then embedded in elastomer matrix to obtain stretchable nanopapers (defined as the stretchable electrode with embedded flexible nanopaper). Crumpled graphene was mixed with nanocellulose (weight ratio 1:1) and vacuum filtrated using polycarbonate (PC) filter membrane (pore size 220 nm). Uniform composite films were obtained after filtration due to the simultaneous extraction of solvent from the evenly distributed track-etched pores in the filter membrane. The film can be peeled off from the filter membrane when dried as a free-standing flexible nanopaper, as shown in Figure 1b-c. Mechanical strength of the composite nanopaper is significantly improved as compared with the loosely packed pure graphene film without nanocellulose addition (Figure S1, Supporting Information), which tend to crack and delaminate from the filter membrane and prohibit their further processing into stretchable form. A graphene to nanocellulose weight ratio of 1:1 (graphene content 50 *wt*%) was found to be suitable for strain sensing applications. No observable performance variations were found when the graphene content was varied in the range of 33 wt% (1:2) and 67 wt% (2:1). However, further variations beyond this range were found to be detrimental to device performances. For example, the nanopaper became quite rigid when the graphene content was decreased to 17 wt% (1:5) and exhibited poor stretchability (easy to crack and fracture). The composite nanopaper behaved like pure graphene film when the graphene content was increased to 83 wt% (5:1) and exhibited poor processability.

The flexible nanopaper was impregnated with polydimethylsiloxane (PDMS) to fabricate stretchable nanopapers.

Dr. C. Y. Yan, J. X. Wang, W. B. Kang, M. Q. Cui, X. Wang, C. Y. Foo, K. J. Chee, Prof. P. S. Lee
School of Materials Science and Engineering
Nanyang Technological University
50 Nanyang Avenue, 639798, Singapore
E-mail: pslee@ntu.edu.sg

DOI: 10.1002/adma.201304742

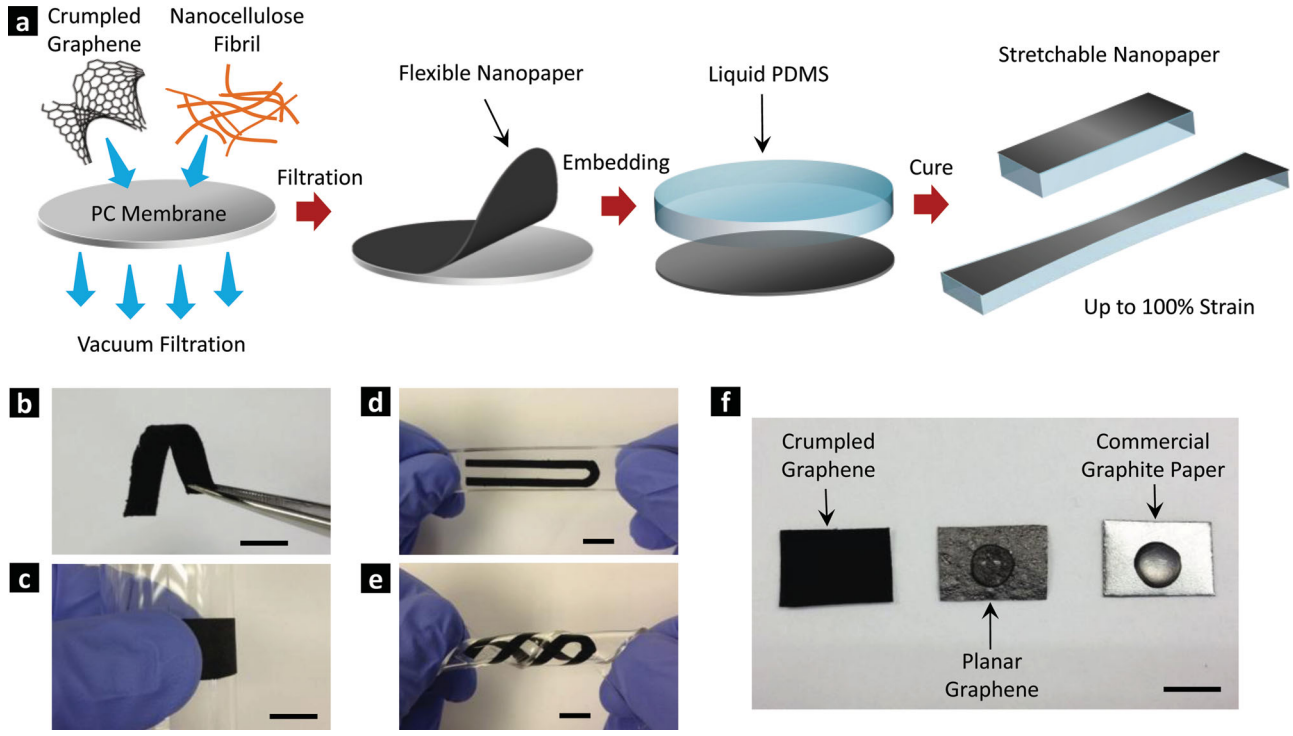

Figure 1. a) Schematic illustrations of the fabrication processes for stretchable graphene nanopapers. b–e) Example images of the free-standing flexible nanopaper (b,c) and stretchable nanopaper (d,e). f) Water adsorption comparison of crumpled graphene paper, planar graphene paper and commercial graphite paper. The scale bars in (b–f) are 10 mm.

Representative images of the stretchable graphene nanopapers are shown in Figure 1d,e. Successful embedding into the elastomer matrix is only possible for the crumpled graphene nanopaper with 3D macroporous structure (**Figure 2**). Figure 1f shows a straightforward comparison demonstrating the structural differences of crumpled graphene nanopaper, planar graphene paper[21] and commercial graphite paper. Deionized (DI) water was dropped on top of the respective paper substrates, and the water droplet on crumpled graphene nanopaper was quickly adsorbed suggesting the porous nature of the nanopaper, however, substrates made of planar graphene and commercial graphite are compact and do not allow efficient liquid penetration (Figure 1f). Fabrication of stretchable graphene structures for high-strain sensors was found to be only feasible for the macroporous nanopaper from crumpled graphene and nanocellulose composite.

Scanning electron microscopy (SEM) characterizations of the flexible and stretchable nanopapers are shown in Figure 2. Top view SEM images (Figure 2a–c) clearly revealed the rough and porous surface of the nanopaper from crumpled graphene. However, SEM characterizations of the planar graphene paper and commercial graphite paper showed compact top surfaces which prohibited elastomer infiltration and embedding (Figure S2, Supporting Information). A representative high-magnification view of the crumpled graphene is shown in Figure 2c. Although the sizes and morphologies of the crumpled graphene are not as uniform as those graphene balls,[22] the heavily wrinkled structures have similar effects in constructing loosely-stacked films with sufficient void spaces for liquid penetration, in contrast to planar graphene paper where

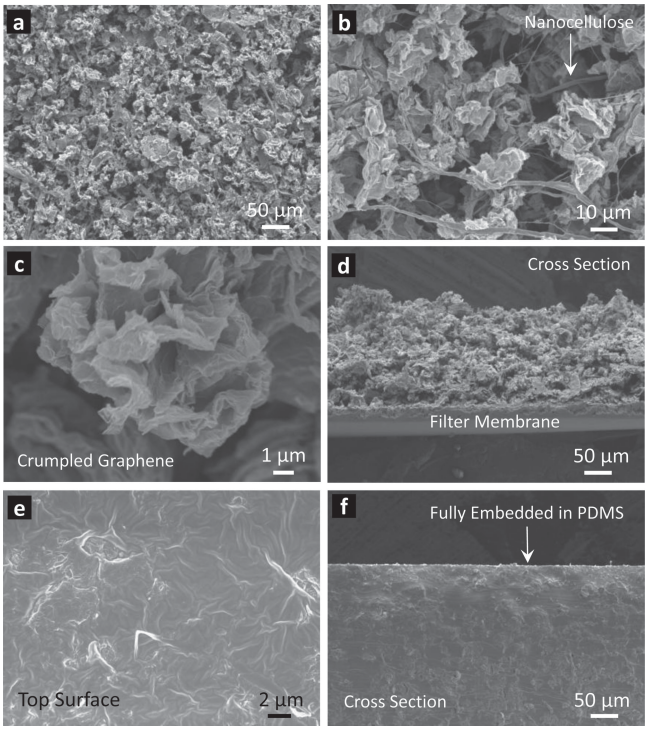

Figure 2. Structural characterizations of the flexible and stretchable nanopapers. a–c) Top view SEM images of flexible nanopaper showing the macroporous structure based on crumpled graphene and nanocellulose. d) Cross-sectional view showing that the flexible nanopaper is porous throughout the entire thickness. e,f) Top view and cross-sectional view of the stretchable nanopaper with fully embedded structure.

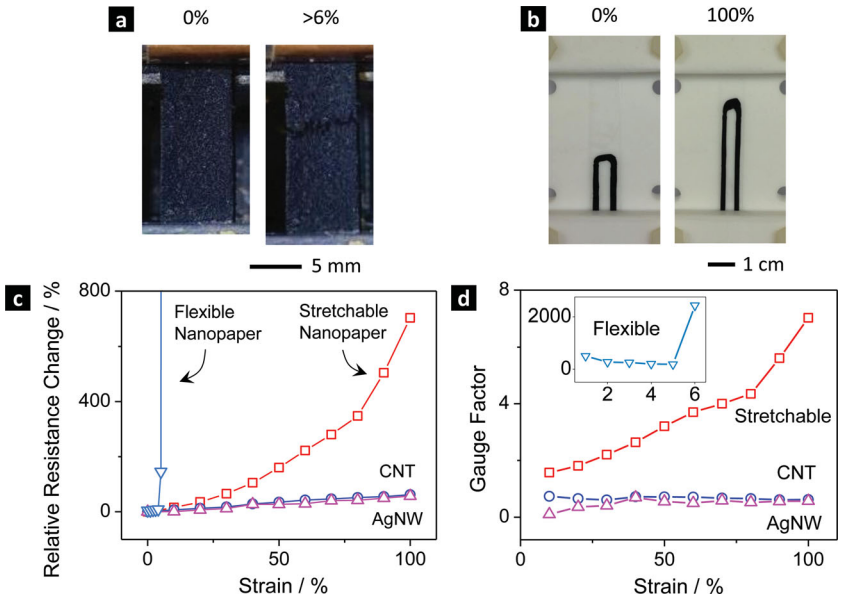

Figure 3. a,b) Flexible nanopaper can only sustain a very limited strain of 6% (a), but stretchable nanopaper can be stretched up to 100% (mechanical fracture limit of the PDMS substrate) (b). c,d) Plots of relative resistance change (c) and gauge factors versus strain (d) for flexible nanopaper, stretchable nanopaper as well as stretchable CNT (blue circles) and AgNW (pink triangles) electrodes.

the flat nanosheets tend to be closely packed to minimize the surface energy.[21,22] Cross-sectional view of the nanopaper is shown in Figure 2d. The nanopaper maintains its porous structure throughout the entire thickness, ensuring that the flexible nanopaper can be fully embedded in the elastomer matrix, which was verified by SEM characterizations of the samples after PDMS infiltration (top view in Figure 2e and cross-sectional view in Figure 2f).

Comparative strain sensing properties of the flexible and stretchable nanopapers are shown in **Figure 3**. Relative resistance changes versus strains are shown in Figure 3c. Nanopapers in flexible form can only be stretched to a very limited extend (maximum 6% strain) and will break upon further stretching (Figure 3a), resulting in an infinite resistance change (Figure 3c). On the contrary, the stretchable nanopaper can be stretched up to 100% without mechanical failure (Figure 3b), a significantly improved stretchability after PDMS embedding. Note that the stretchability is only limited by the mechanical fracture limit of PDMS, which is thickness-dependent[23–25] and was found to be ca. 100% for substrates of 1 mm thick in our case. The stretchability can be further improved by using elastomer substrates with higher stretchability such as Ecoflex which can be stretched to 300%.[26] A relative resistance change $[(R - R_0)/R_0$, R_0 is the resistance at 0% strain] of 710% was observed at 100% strain for stretchable nanopapers. 1D nanostructures such as carbon nanotubes (CNTs) and silver nanowires (AgNWs) were widely used as elastic conductors in stretchable electronics.[4,24,25,27] For comparison, stretchable CNT and AgNW electrodes with fully embedded structures (Figure S3, Supporting Information) were also fabricated and compared with graphene nanopaper, as shown in Figure 3c. The relative resistance changes of CNT and AgNW electrodes are much less prominent than stretchable graphene nanopaper and only ca. 60% resistance changes were observed at 100% strain. While it is desirable to minimize the resistance changes upon stretching when they are used as electrodes to maintain consistent device performances, the requirements are essentially the opposite for strain sensor applications, where higher resistance changes are pursued to improve the sensitivity. We suggest that stretchable graphene nanopapers with >10 times higher relative resistance change (at 100% strain) are superior candidates for strain sensing applications, considering the significantly improved piezoresistive responses than their 1D counterparts such as CNTs and AgNWs.

Piezoresistive effects of elastic conductors arise primarily from two aspects:[28] i) intrinsic piezoresistivity of the filler; ii) piezoresistivity due to the change of the contact conditions for electron conduction, such as break of contacts, contact area and spacing variations upon stretching, etc. The intrinsic piezoresistivity of monolayer and few-layer graphene has been demonstrated.[15,29] However, the hexagonal mesh of graphene can only be stretched to ca. 6% before fracture[15] thus the intrinsic piezoresistivity will not be the dominant effect for our stretchable nanopapers with ultrahigh stretchability up to 100%. The stretchable graphene nanopaper is composed of stacked crumpled graphene with quasi-spherical morphology. The graphene "spheres" separate apart from each upon stretching, leading to smaller contact areas, larger interspacings or even break of contacts at high strains, all of which contributes to the resistance increase upon stretching. The distinct piezoresistive behaviors of CNT and AgNW elastic conductors can be understood based on the structure-dependent percolative contacting behaviors. CNTs and AgNWs in the percolative film have much more contacting nodes with each other owing to the high aspect ratio of 1D structures. Upon stretching, the strains can be efficiently accommodated by the intersliding and rearrangement of NWs but meanwhile sufficient contacting nodes are well maintained. Consequently, smaller resistance changes were observed for CNT and AgNW elastic conductors as compared with graphene nanopapers.

Gauge factor is a characteristic parameter representing the sensitivity of the strain sensors and can be derived from $(R - R_0)/(R_0\varepsilon)$, where ε is the strain. Gauge factors as a function of strains for the four types of elastic electrodes are shown in Figure 3d. The gauge factors for stretchable nanopaper increased from 1.6 at 10% strain to 7.1 at 100% strain. The relatively higher gauge factor upon further stretching arises from the more severe separation between crumpled graphene at higher strain. However, the stretchable CNT and AgNW electrodes maintained relatively low gauge factors (ca. 0.65 for CNT and ca. 0.5 for AgNW) within the strains of 0–100%. Although flexible nanopapers exhibit much higher gauge factors from 502 at 1% strain to 2427 at 6% strain (Figure 3d inset), the

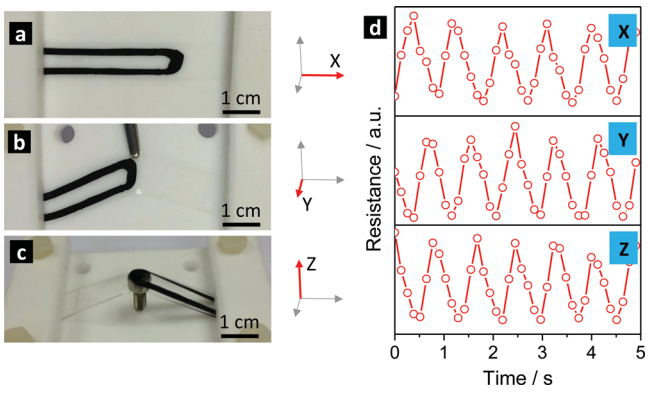

Figure 4. a–c) Example images of the graphene nanopaper sensors stretched in the X-, Y- and Z directions. d) Corresponding response curves for stretching in three directions.

limited stretchability (6%) restricts their applications for high-strain detections. The gauge factors for our stretchable graphene nanopaper (achieved >7 at 100% strain) are comparable with previous graphene-based strain sensors. For example, buckled graphene on elastomer substrates (stretchability 25–30%) exhibited gauge factors in the range of 2–4.[15,16] Graphene foam showed a gauge factor of ca. 2 at the maximum strain.[13] Higher gauge factors were reported but only for devices with very limited stretchability, analogous to our flexible nanopaper. For example, a gauge factor of 300 was reported for nanographene film deposited on mica substrate, although the stretching limit was as low as 0.4%.[17]

The stretchable graphene nanopaper sensors are capable of all-directional sensing. Example images showing the strains from the X, Y and Z directions are shown in **Figure 4**a–c, respectively. Corresponding response behaviors of the strain sensors are shown in Figure 4d. Efficient tracing and detection of strain variations from all directions is evident. The soft nature of elastomer substrates allows the deformation and hence successful detection of strains from all directions, which is of critical importance for applications like human-motion detection. For example, the simple movements of human fingers would naturally generate strain from three dimensions. However, proper 3D strain detection cannot be achieved using conventional strain sensors based on metal and semiconductors or previous graphene sensors based on flexible but not stretchable substrates.[30] The capability of all-directional sensing also allows the efficient detection of a variety forms of forces beyond uniaxial strain, such as torsion force, shearing force, compression force, etc.[31]

Application of the graphene strain sensors for human-motion detection is demonstrated. The proof-of-concept device includes five independent sensors implanted on a feather glove to detect the bending and stretching of fingers. An overview image of the data glove and images showing the stretching and bending states of fingers are shown in **Figure 5**a. The sensors were designed into U-shaped to facilitate electrical measurements. Figure 5b shows the response behaviors of the strain sensors when the fingers were repeatedly bended and stretched at a frequency of 1 Hz. Measured strains for the five independent strain sensors during finger movements lied in the range of 35–45%. Proper functioning of the graphene elastic conductors for efficient human-motion detections are clearly visible. Human-interactive electronics based on unconventional stretchable and wearable technologies have attracted considerable attention recently.[20,32–35] Our data glove based on stretchable graphene nanopaper represents an important branch of electromechanical devices and can be used for fine-motion control in robotics and other virtual realities. Existing interactive data gloves mainly rely on sensing elements of optical fibers or metal strain gauges.[36] However, our innovative graphene devices are advantageous in terms of fabrication costs and complexity, and they do not impose stretchability limits of the motion of the hands.

Our strategy for the successful fabrication of highly stretchable graphene nanopapers presents several key advancements: i) graphene with unique crumpled morphologies was shown to be essential for successful embedding into elastomer matrix. The fabrication of stretchable graphene sensors is only feasible for crumpled graphene film with 3D macroporous structure. The compact surfaces of planar graphene paper or commercial

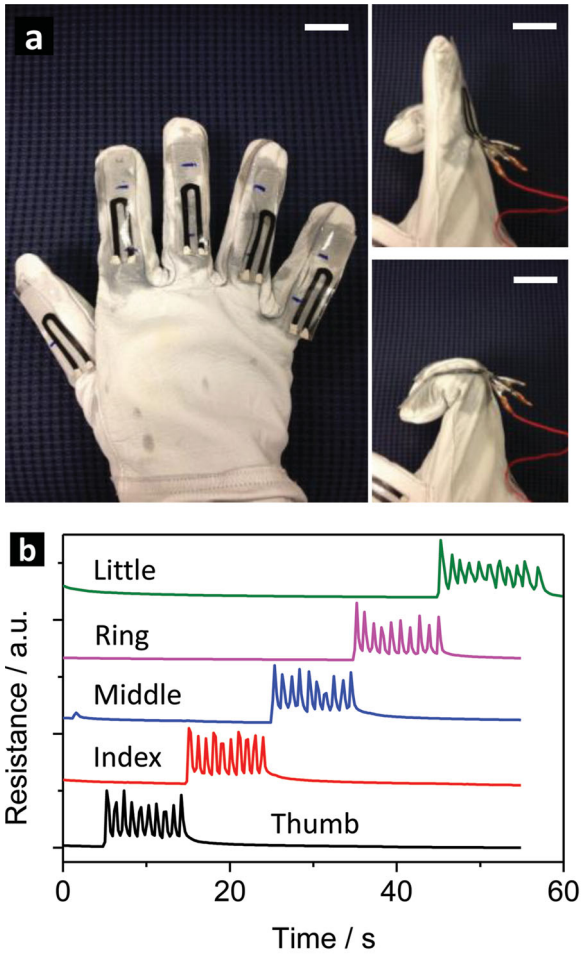

Figure 5. Wearable strain sensors for finger movement detections. a) Photographs of the data glove with five implanted sensors. The bending and stretching states of the glove finger during testing are also shown. Scale bars: 2 cm. b) Relative resistance changes for the five independent strain sensors.

graphite paper do not allow facile liquid infiltration and thus cannot be embedded in elastomer matrix to obtain stretchable structures. ii) Nanocellulose was found to be an efficient, low-cost and green "binder" to enhance the processability of crumpled graphene. Unlike bulky paper from close-packed planar graphene flakes,[21] crumpled graphene has much weaker interactions due to the quasi-spherical morphologies[22] and the filtered film cannot be picked up as a free-standing paper. We have shown that the mechanical strength can be significantly improved with the addition of nanocellulose. The enhancement effects primarily originate from the physical binding forces of the 1D nanocellulose fibrils since 1D nanostructures within an entangled film (such as CNT bulky paper)[37] were shown to have strong mechanical interactions. Contributions of chemical binding forces between the surface functional groups[38] are expected to play a less dominant role considering the limited contact areas of nanocellulose fibrils and crumpled graphene, as shown in Figure 2b. iii) The stretchable graphene nanopapers are >10 times more sensitive than devices based on 1D nanomaterials such as CNTs and AgNWs. While there are significantly more contacting nodes in the percolating networks of 1D nanomaterials, they show less prominent resistance change upon stretching as compared with crumpled graphene. iv) Compared with conventional strain sensors, our graphene nanopapers have much higher strain detection limits and are capable of all-directional strain sensing, which are critical requirements for emerging human-interactive applications. v) Our methodology yields graphene nanopapers that can be stretched up to 100% and was only limited by the stretchability of PDMS substrate. There are very few reports on graphene strain sensors that are capable for the detection of high-strain exceeding 50%. Representative reports on graphene strain sensors are summarized in **Table 1** (refer to Table S1 in Supporting Information for more references). Graphene foam[13] exhibited a stretchability of 95%, but the fabrication method is expensive, time-consuming and low yield. We show that high performance strain sensors can be produced in a low-cost, facile, and scalable manner with solution-processable graphene and nanocellulose.

In conclusion, we report an innovative method for the fabrication of high-strain sensors based on crumpled graphene and nanocellulose. Free-standing flexible nanopapers were fabricated using vacuum filtration method and the 3D macroporous structure enables their successful embedding in elastomer matrix to obtain stretchable nanopapers. The stretchability was successfully improved from 6% for flexible nanopaper to 100% for stretchable nanopaper. The high-strain sensors based on stretchable nanopaper exhibited a gauge factor of 7.1 at 100% strain, which is >10 times higher than stretchable CNT and AgNW sensors. Compared with conventional metal and semiconductor based devices, the stretchable nanopaper sensor also allows all-directional sensing which is critical for efficient human-motion detections. Prototype devices were also demonstrated by implanting graphene nanopaper sensors on data gloves for finger movement detection. The facile, low cost and readily scalable method allows practical fabrication of graphene high-strain sensors for emerging human-interactive applications.

Table 1. Maximum strains of graphene-based strain sensors.

Strain Sensors	Max Strain [%]	Ref.
Graphene-PVDF composite	0.1	[39]
Graphene nanoplatelets-CNT composite	0.2	[30]
Few-layer graphene	1	[40]
Percolative graphene film	1.7	[14]
Suspended graphene nanoribbon	3	[41]
Graphene monolayer	4.5	[42]
Graphene ripple	30	[15]
Graphene foam	95	[13]
Graphene nanopaper	100	This work

Experimental Section

Flexible Nanopaper: Crumpled graphene is commercially available and used as received (Time Nano, China, product number: TNRGO, thickness 0.5–3.74 nm, flake size 0.5–3 μm, purity >99 wt%, specific surface area 500–1000 $m^2\ g^{-1}$). The fabrication method for crumpled graphene is briefly described as below. Graphene oxide sheets were first prepared from natural graphite flakes using modified Hummers method.[43] The graphene oxide dispersion (in aqueous solution) was dried in a vacuum oven until the water content dropped to ca. 10–20 wt% and then placed into a quartz tube furnace kept at 1200 °C with inert N_2 atmosphere. The graphene oxide was reduced at 1200 °C for 5 min before moved to the room temperature region of the quartz tube furnace. The crumpled morphologies are likely to be induced by the capillary compression forces of water during the drying processes, as have also been observed in previous report where heavily crumpled graphene balls were obtained by the rapid drying of aerosol droplets containing graphene.[22] Nanocellulose fibril (The University of Maine, Process Development Center, USA, diameter 20 nm, length 1 μm) was dispersed in aqueous solution with a concentration of 3 wt%. As-received graphene and nanocellulose was mixed in DI water (weight ratio 1:1) and stirred at 500 rpm for 10 min. The mixture solution was then filtered using PC filter membranes (Millipore GTTP, pore size = 220 nm) to get a uniform flexible nanopaper. The nanopaper was rinsed with ethanol (99.9%, Merck KGaA, Germany) after filtration. The nanopaper on filter membrane was leave in air at room temperature for 30 min to dry. The flexible nanopaper can be separated from the filter membrane to obtain free-standing film.

Stretchable Nanopaper: The flexible nanopaper on filter membrane was put in a glass petri dish for PDMS infiltration. The PDMS base and curer (Sylgard 184, Dow Corning, USA) was mixed (weight ratio = 10:1) and poured on top of the flexible nanopaper. The petri dish was then degassed in a vacuum desiccator for 30 min to allow sufficient PDMS infiltration before curing at 60 °C for 2 h. The solidified PDMS substrate was peeled off from the filter membrane and the flexible nanopaper was successfully embedded into the PDMS elastomer matrix.

Comparative Samples: The detailed fabrication methods of planar graphene paper can be found in our previous work.[21] The commercial graphite paper was purchased from AGM Corp, China (natural graphite >99.95%, thickness 0.5 mm) and used as received. Surface-functionalized CNT was purchased from Time Nano, China (Product Number: TNGMC2, purity >99.9 wt%, –COOH content 1.28 wt%, diameter 8–15 nm, length ca. 50 μm, specific surface area >100 $m^2\ g^{-1}$). The CNTs were dispersed in ethanol with a concentration of 0.5 mg mL^{-1} for filtration. AgNWs were purchased from Seashell Technology LLC, USA (diameter 100 nm, length 20–50 μm, dispersed in isopropyl alcohol, 1 mg mL^{-1}). The CNT and AgNW solutions were filtered and embedded in PDMS matrix using a similar method as crumpled graphene.

Data-Glove Fabrication: The data glove was fabricated by implanting five stretchable graphene nanopaper sensors on the fingers of the glove (Brand: Safewear, goatskin argon leather glove). PDMS liquid was used to "glue" the stretchable nanopaper sensors to the glove surface. The graphene strain sensors were designed into U-shaped so that the two electrical contacts can be connected on one end, which helps to maintain stable connections when the fingers were repeated bended and stretched.

Characterization: The microstructures of the electrodes were characterized using field-emission SEM (FE-SEM) (JSM 7600F, Japan). For the stretching tests, the samples were fixed on home-built stretching stages to apply the desired strain. The relative resistance changes upon stretching were measured using a Keithley analyzer (Model 4200).

Supporting Information

Supporting Information is available from the Wiley Online Library or from the author.

Acknowledgements

This work was supported in part by the Singapore National Research Foundation (CREATE Programme of Nanomaterials for Energy and Water Management). The authors thank X. W. Lu and X. W. Yan for their technical support and insightful discussions.

Received: September 21, 2013
Revised: October 16, 2013
Published online: December 17, 2013

[1] *World Stress/Strain Measurement Equipment Markets*, Frost & Sullivan Research Service, Mountain View, CA, USA **2007**.
[2] A. A. Barlian, W. T. Park, J. R. Mallon, A. J. Rastegar, B. L. Pruitt, *Proc. IEEE* **2009**, *97*, 513.
[3] J. C. F. Millett, N. K. Bourne, Z. Rosenberg, *J. Phys. D* **1996**, *29*, 2466.
[4] T. Yamada, Y. Hayamizu, Y. Yamamoto, Y. Yomogida, A. Izadi-Najafabadi, D. N. Futaba, K. Hata, *Nat. Nanotechnol.* **2011**, *6*, 296.
[5] J. Herrmann, K. H. Muller, T. Reda, G. R. Baxter, B. Raguse, G. de Groot, R. Chai, M. Roberts, L. Wieczorek, *Appl. Phys. Lett.* **2007**, *91*, 183105.
[6] X. Xiao, L. Y. Yuan, J. W. Zhong, T. P. Ding, Y. Liu, Z. X. Cai, Y. G. Rong, H. W. Han, J. Zhou, Z. L. Wang, *Adv. Mater.* **2011**, *23*, 5440.
[7] J. Zhao, G. Y. Zhang, D. X. Shi, *Chin. Phys. B* **2013**, *22*, 057701.
[8] A. K. Geim, K. S. Novoselov, *Nat. Mater.* **2007**, *6*, 183.
[9] K. S. Novoselov, A. K. Geim, S. V. Morozov, D. Jiang, Y. Zhang, S. V. Dubonos, I. V. Grigorieva, A. A. Firsov, *Science* **2004**, *306*, 666.
[10] C. Lee, X. Wei, J. W. Kysar, J. Hone, *Science* **2008**, *321*, 385.
[11] A. Politano, A. R. Marino, D. Campi, D. Farías, R. Miranda, G. Chiarello, *Carbon* **2012**, *50*, 4903.
[12] S. H. Bae, Y. Lee, B. K. Sharma, H. J. Lee, J. H. Kim, J. H. Ahn, *Carbon* **2013**, *51*, 236.
[13] Z. P. Chen, W. C. Ren, L. B. Gao, B. L. Liu, S. F. Pei, H. M. Cheng, *Nat. Mater.* **2011**, *10*, 424.
[14] M. Hempel, D. Nezich, J. Kong, M. Hofmann, *Nano Lett.* **2012**, *12*, 5714.
[15] K. S. Kim, Y. Zhao, H. Jang, S. Y. Lee, J. M. Kim, K. S. Kim, J. H. Ahn, P. Kim, J. Y. Choi, B. H. Hong, *Nature* **2009**, *457*, 706.
[16] Y. Wang, R. Yang, Z. W. Shi, L. C. Zhang, D. X. Shi, E. Wang, G. Y. Zhang, *ACS Nano* **2011**, *5*, 3645.
[17] J. Zhao, C.L. He, R. Yang, Z. W. Shi, M. Cheng, W. Yang, G. B. Xie, D. M. Wang, D. X. Shi, G. Y. Zhang, *Appl. Phys. Lett.* **2012**, *101*, 063112.
[18] T. Yu, Z. Ni, C. Du, Y. You, Y. Wang, Z. Shen, *J. Phys. Chem. C* **2008**, *112*, 12602.
[19] D. Y. Khang, H. Q. Jiang, Y. Huang, J. A. Rogers, *Science* **2006**, *311*, 208.
[20] J. A. Rogers, T. Someya, Y. G. Huang, *Science* **2010**, *327*, 1603.
[21] A. Sumboja, C. Y. Foo, X. Wang, P. S. Lee, *Adv. Mater.* **2013**, *25*, 2809.
[22] J. Luo, H. D. Jang, T. Sun, L. Xiao, Z. He, A. P. Katsoulidis, M. G. Kanatzidis, J. M. Gibson, J. Huang, *ACS Nano* **2011**, *5*, 8943.
[23] L. Cai, J. Li, P. Luan, H. Dong, D. Zhao, Q. Zhang, X. Zhang, M. Tu, Q. Zeng, W. Zhou, S. Xie, *Adv. Funct. Mater.* **2012**, *22*, 5238.
[24] F. Xu, Y. Zhu, *Adv. Mater.* **2012**, *24*, 5117.
[25] D. J. Lipomi, M. Vosgueritchian, B. C. K. Tee, S. L. Hellstrom, J. A. Lee, C. H. Fox, Z. N. Bao, *Nat. Nanotechnol.* **2011**, *6*, 788.
[26] S. Xu, Y. H. Zhang, J. Cho, J. Lee, X. Huang, L. Jia, J. A. Fan, Y. W. Su, J. Su, H. G. Zhang, H. Y. Cheng, B. W. Lu, C. J. Yu, C. Chuang, T. I. Kim, T. Song, K. Shigeta, S. Kang, C. Dagdeviren, I. Petrov, P. V. Braun, Y. G. Huang, U. Paik, J. A. Rogers, *Nat. Commun.* **2013**, *4*, 1543.
[27] S. Yun, X. F. Niu, Z. B. Yu, W. L. Hu, P. Brochu, Q. B. Pei, *Adv. Mater.* **2012**, *24*, 1321.
[28] C. Lee, L. Jug, E. Meng, *Appl. Phys. Lett.* **2013**, *102*, 183511.
[29] S.-H. Bae, Y. Lee, B. K. Sharma, H.-J. Lee, J.-H. Kim, J.-H. Ahn, *Carbon* **2013**, *51*, 236.
[30] S. Luo, T. Liu, *Adv. Mater.* **2013**, *25*, 5660.
[31] X. Li, R. Zhang, W. Yu, K. Wang, J. Wei, D. Wu, A. Cao, Z. Li, Y. Cheng, Q. Zheng, R. S. Ruoff, H. Zhu, *Sci. Rep.* **2012**, *2*, 870.
[32] D. H. Kim, N. S. Lu, R. Ma, Y. S. Kim, R. H. Kim, S. D. Wang, J. Wu, S. M. Won, H. Tao, A. Islam, K. J. Yu, T. I. Kim, R. Chowdhury, M. Ying, L. Z. Xu, M. Li, H. J. Chung, H. Keum, M. McCormick, P. Liu, Y. W. Zhang, F. G. Omenetto, Y. G. Huang, T. Coleman, J. A. Rogers, *Science* **2011**, *333*, 838.
[33] M. Park, J. Im, M. Shin, Y. Min, J. Park, H. Cho, S. Park, M. B. Shim, S. Jeon, D. Y. Chung, J. Bae, U. Jeong, K. Kim, *Nat. Nanotechnol.* **2012**, *7*, 803.
[34] T. Sekitani, H. Nakajima, H. Maeda, T. Fukushima, T. Aida, K. Hata, T. Someya, *Nat. Mater.* **2009**, *8*, 494.
[35] C. Wang, D. Hwang, Z. Yu, K. Takei, J. Park, T. Chen, B. Ma, A. Javey, *Nat. Mater.* **2013**, *12*, 899.
[36] L. Dipietro, A. M. Sabatini, P. Dario, *IEEE Trans. Syst. Man Cybernetics* **2008**, *38*, 461.
[37] M. Endo, H. Muramatsu, T. Hayashi, Y. A. Kim, M. Terrones, M. S. Dresselhaus, *Nature* **2005**, *433*, 476.
[38] L. Hu, M. Pasta, F. L. Mantia, L. Cui, S. Jeong, H. D. Deshazer, J. W. Choi, S. M. Han, Y. Cui, *Nano Lett.* **2010**, *10*, 708.
[39] V. Eswaraiah, K. Balasubramaniam, S. Ramaprabhu, *Nanoscale* **2012**, *4*, 1258.
[40] Y. Lee, S. Bae, H. Jang, S. Jang, S.-E. Zhu, S. H. Sim, Y. I. Song, B. H. Hong, J.-H. Ahn, *Nano Lett.* **2010**, *10*, 490.
[41] M. Huang, T. A. Pascal, H. Kim, W. A. Goddard, J. R. Greer, *Nano Lett.* **2011**, *11*, 1241.
[42] X.-W. Fu, Z.-M. Liao, J.-X. Zhou, Y.-B. Zhou, H.-C. Wu, R. Zhang, G. Jing, J. Xu, X. Wu, W. Guo, D. Yu, *Appl. Phys. Lett.* **2011**, *99*, 213107.
[43] N. I. Kovtyukhova, P. J. Ollivier, B. R. Martin, T. E. Mallouk, S. A. Chizhik, E. V. Buzaneva, A. D. Gorchinskiy, *Chem. Mater.* **1999**, *11*, 771.